Available online at www.sciencedirect.com

ScienceDirect

Procedia Computer Science 90 (2016) 54 – 60

Procedia Computer Science

International Conference On Medical Imaging Understanding and Analysis 2016, MIUA 2016, 6-8 July 2016, Loughborough, UK

Automatic Generation of Synthetic Retinal Fundus Images: Vascular Network

Lorenza Bonaldi[a], Elisa Menti[a], Lucia Ballerini[b,*], Alfredo Ruggeri[c], Emanuele Trucco[a]

[a] *VAMPIRE project, Computing, School of Science and Engineering, University of Dundee, UK*
[b] *VAMPIRE project, Department of Neuroimaging Sciences, University of Edinburgh, UK*
[c] *Department of Information Engineering, University of Padova, Italy*

Abstract

This work is part of an ongoing project aimed to generate synthetic retinal fundus images. This paper concentrates on the generation of synthetic vascular networks with realistic shape and texture characteristics. An example-based method, the Active Shape Model, is used to synthesize reliable vessels' shapes. An approach based on Kalman Filtering combined with an extension of the Multiresolution Hermite vascular cross-section model has been developed for the simulation of vessels' textures. The proposed method is able to generate realistic synthetic vascular networks with morphological properties that guarantee the correct flow of the blood and the oxygenation of the retinal surface observed by fundus cameras. The validity of our synthetic retinal images is demonstrated by qualitative assessment and quantitative analysis.

Peer-review under responsibility of the Organizing Committee of MIUA 2016

Keywords: Synthetic Retinal Images, Shape, Texture, Validation

1. Introduction

Retinal Image Analysis (RIA) aims to develop computational and mathematical techniques for helping clinicians with the diagnosis of diseases such as diabetes, glaucoma and cardiovascular conditions, that may cause changes in retinal blood vessel patterns like tortuosity, bifurcations, variation of vessel width and colour[1,2]. RIA algorithms have to be validated to avoid obtaining misleading results. Validation can be defined as the process of showing that an algorithm performs correctly by comparing its output with a reference standard[3]. A common practice for validation of medical image algorithms is to use Ground Truth (GT) provided by medical experts. Obtaining manually GT images annotated by clinicians is an expensive and laborious task which motivates the creation of a synthetic dataset providing GT for algorithm validation. Medical phantoms are extensively used in many medical imaging environments[4,5]. However, to our best knowledge, there are no publicly available databases of synthetic retinal fundus images, and providing annotations for large image repositories (e.g. UK Biobank alone stores fundus images for

* Corresponding author. Tel.: +44-131-4659529 – Bonaldi and Menti contributed equally
E-mail address: lucia.ballerini@ed.ac.uk

Peer-review under responsibility of the Organizing Committee of MIUA 2016
doi:10.1016/j.procs.2016.07.010

68,000 patients) is often impossible. Synthesized high-resolution fundus images, along with GT free from inter-/ intra-observer variability, would allow an efficient validation of algorithms for segmentation and analysis of retinal anatomical structures: by tuning morphological and textural characteristics of these images, we can represent the hallmarks of several diseases or different populations. This work focuses on the generation of retinal vessels and their integration with non-vessel regions to yield complete fundus camera images, i.e. retinal background, fovea and Optic Disc (OD), previously reported by Fiorini et al.[6]. The resulting synthetic retinal fundus images include explicit GT for vessels binary maps, bifurcation point locations, vessel widths and artery/vein classification.

This paper is organized as follows. In Section 2 we describe the proposed method for the generation of the morphological properties (Subsection 2.2) and the textural features (Subsection 2.3) of the vasculature. In Section 3 we report results and summarize and discuss our experiments to evaluate them. Finally in Section 4 we give concluding remarks and hints for future work.

2. Method

2.1. Overview

The proposed approach consists of a learning phase and a generation phase. In the former phase, data describing vascular morphology and texture are collected from annotations of real images. Models are specified and their parameters learned from the training data. In the latter phase, the models obtained are used to create synthetic vascular networks. Arteries (A) and Veins (V) are created separately with the same protocol, and then combined together. This work is based on the publicly available High-Resolution Fundus[1] (HRF) images database[7], and on a subset of retinal images of the GoDARTS bioresource [2].

2.2. Vascular Morphology

The generation of synthetic vessel morphology has been achieved using the well-known Active Shape Model (ASM)[8]. This model provides a statistical representation of shape represented by a set of points, called *landmark points*. By analysing the variations in shape over the training set, a PCA model is built. The training samples (vessel shapes in our case) are aligned into a common coordinate frame and the deviations from the mean shape are analysed. Each training shape is represented as a fixed number n of landmark points placed along a vessel and equally spaced. These landmarks form a $2n$ vector $\mathbf{x}$, the dimensionality of which is reduced using Principal Component Analysis (PCA), assuming that the most interesting feature is the one with the largest variance. Hence, each shape can be approximated as:

$$\mathbf{x_i} \approx \bar{\mathbf{x}} + \mathbf{P}\mathbf{b_i} \tag{1}$$

where $\bar{\mathbf{x}}$ is the mean shape of the aligned data, $\mathbf{P}$ contains the first t eigenvectors corresponding to the largest t eigenvalues of the covariance matrix of the training shapes, and $\mathbf{b_i}$ is a t dimensional vector of parameters of a deformable shape model. We choose t, so that the model represents 98% of the total variance of our training data. By varying the element in $\mathbf{b_i}$, randomly choosing them from a multivatiate normal distribution learned across the training set shapes, we generate a new synthetic vessel using Eq. (1).

The data describing the shape of the vessels of each type (A and V) for the main arcades, nasal and temporal ($n = 81$ landmarks), and their branches ($n = 31$ landmarks) up to three levels of branching have been previously collected from 50 GoDARTS retinal fundus images. We used the polar coordinate system centred in the OD and having the main axis in the direction of the OD-Fovea axis (i.e. the line connecting the OD centre and the fovea), adopted by the VAMPIRE software suite[9]. Vessel shapes are represented into this system using a transformation that includes a rigid translation and rotation. Fig. 1 (a) shows the aligned set of shapes of the temporal arcades and their mean shape. Similarly the shapes of the branches have been aligned using a rigid transformation that shifts their starting point to the origin of the same coordinate system.

[1] The HRF database can be free downloaded at http://www5.cs.fau.de/research/data/fundus-images/
[2] The GoDARTS resource is described at http://medicine.dundee.ac.uk/godarts

Individually generated synthetic vessels are then connected to create the vascular network skeleton. The location of vessel bifurcations is estimated from real images as follows. First we calculate the spatial density distribution map (Fig. 1 (b)) of all bifurcation points annotated on real images. Then we map our synthetic vessel onto it, obtaining a probability score for each point of the vessel to become a bifurcation point (Fig. 1 (c)). We select one of the points having maximum score as the first bifurcation point of the main arcades. We select the following bifurcation point as one of the points having maximum score located at a distance $d \in [l/2n, l/n]$ from the previous one, where l is the length of the vessel and n is the desired number of bifurcations. We continue to select points until reaching the desired number of bifurcation points.

For each branch originating from a bifurcation point we compute its orientation and calibre using the bifurcation model described by Murray's Law[10], linking branching angles with vessel calibres. Newly generated synthetic branches need to fit with the context of the vascular tree already generated: all vessels should be inside the Field of View (FOV), but outside the foveal region, avoiding intersections between vessels of the same type, and converging toward the fovea.

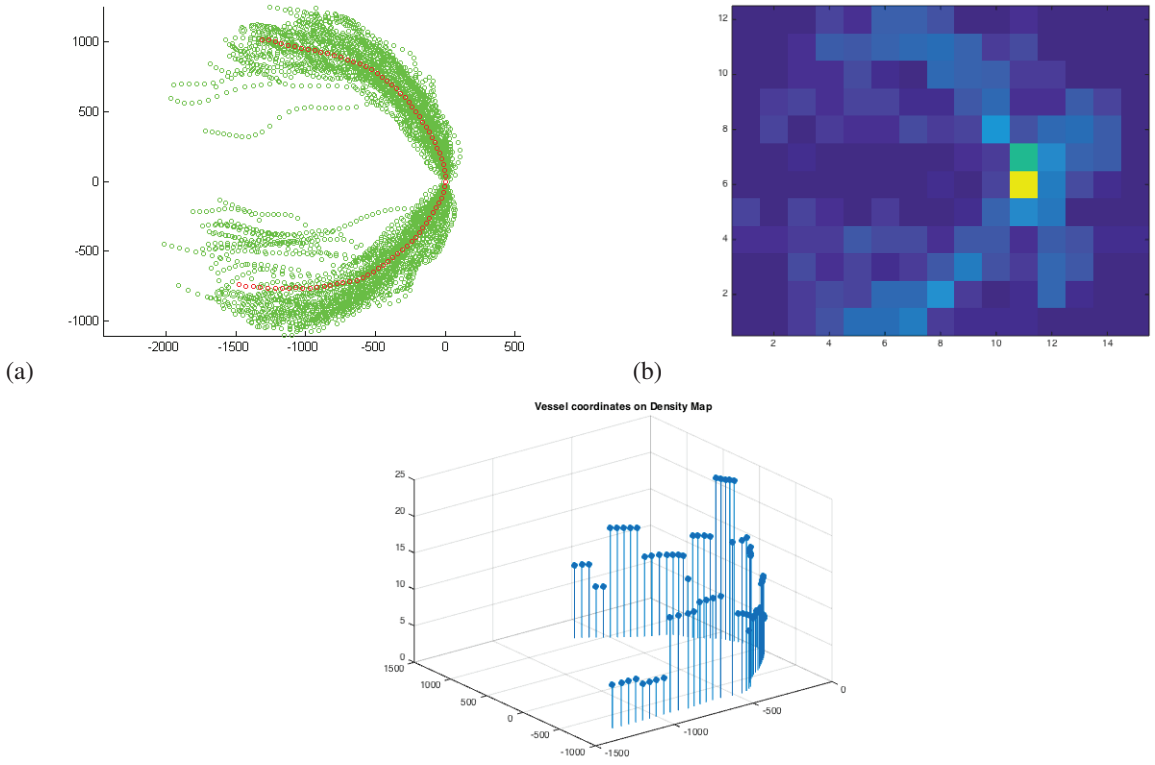

Fig. 1. (a) Aligned shapes of the temporal arcades (green) and their mean shape (red). (b) Density Map distribution of artery bifurcation points in the image plane. (c) A synthetic vessel with the probability score of each point to be a bifurcation point.

The binary map of the vascular tree (shown in Fig. 2) is obtained by adding calibre information using mathematical morphological dilation of the skeleton. The initial calibre of the main arcades is sampled from the estimate distribution of the largest vessel calibre of real images. The branches initial calibre is obtained from the parent vessel calibre according to Murray's Law.

2.3. Vascular Texture

To generate synthetic vessel textures we collected information of the intensity values along vessels and textural features of the surrounding area (background), we created a model that combines these two sets of information capturing the transition of intensities between vessels and background.

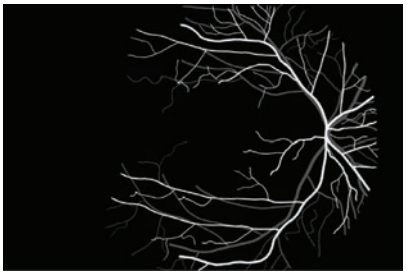

Fig. 2. Example of synthetic vascular tree (arteries in white and veins in gray for display purpose).

2.3.1. Data Collection

Cross-sections of the vessel of interest were defined, spaced by 5 pixels along the vessel centerline. We extracted the intensity RGB profile on lines perpendicular to the direction of the vessel as depicted in Fig. 3 (a). The green channel intensities are fitted (Fig. 3 (b)) with a weighted NonLinear Least Squares model using a 6-parameters Extended Multiresolution Hermite Model[11] (EMHM) to fit the cross-sectional intensity profiles. The EMHM accounts for non-symmetric and symmetric profiles, with or without central reflex, expressed by the formula:

$$H(a, m, \delta, \sigma, p, q, x) = -p\{1 + a[(x - m - \delta)^2 - 1]\}e^{-\frac{(x-m)^2}{2\sigma^2}} + q \tag{2}$$

where $a \in [-1, 1]$ models the depth of the central reflection; $m \in [1, \textit{length(profile)}]$ is the mean of the Gaussian and allows shifts along the x-axis and *length(profile)* is the length of the vessel region around the target location; $\delta \in [-2, 2]$ accounts for asymmetry; $\sigma \in [1, 15]$ is the standard deviation of the Gaussian; $q \in [0, 255]$ shifts the function along the y-axis, avoiding negative pixel values; $p \in [0, 150]$ guarantees that vessels are darker than the background; x is a vector of the same length of the cross-section of the vessel. The initial conditions are $a = 0$, $m = \textit{length(profile)}/2$, $\delta = 0.2$, $\sigma = \textit{length(profile)}/\textit{std(profile)}$, $q = \textit{max(profile)}$, $p = \textit{max(profile)} - \textit{min(profile)}$.

At the extremities of each cross-section (green circles in Fig. 3 (a)) we computed five statistical texture descriptors[12,13] (Mean, Std, Skewness, Kurtosis and Entropy) on two near-circular windows of 6 pixel radii.

The ensemble of these data, 6 EMHM parameters ($\mathbf{X}_{n\times 6}$) and 5×2 background texture descriptors ($\mathbf{Y}_{n\times 10}$) for each profile, for a total of 975 artery and 1593 vein profiles, collected from the 15 healthy subjects of the HRF dataset, constitute the measurements for the procedure proposed below.

2.3.2. Generation of Vessel Textures

The procedure for creating reliable synthetic vessel texture takes into account both the continuity of intensity profiles along the vessel and their consistence with background intensities. We apply a Kalman Filter[14], we formulate our problem as a state space system:

$$\begin{cases} \mathbf{x}_k = \mathbf{F}\mathbf{x}_{k-1} + \mathbf{w}_{k-1} & \text{System model} \\ \mathbf{y}_k = \mathbf{H}\mathbf{x}_k + \mathbf{v}_k & \text{Measurement model} \end{cases} \tag{3}$$

where $\mathbf{x}_k$ is the state vector containing the 6 parameters describing the intensity profile, $\mathbf{F}$ is the state transition matrix (set to identity matrix), $\mathbf{y}_k$ is the vector of measurements given by 10 textural descriptors of the synthetic background and the two vectors $\mathbf{w}_{k-1}$ and $\mathbf{v}_k$ are unrelated realizations of white zero-mean Gaussian noise. The measurement matrix $\mathbf{H}$ has been obtained, using Multivariate Multiple Linear Regression, solving the system:

$$\begin{bmatrix} y_{1,1} & \dots & y_{1,10} \\ \vdots & \ddots & \vdots \\ y_{n,1} & \dots & y_{n,10} \end{bmatrix} = \begin{bmatrix} x_{1,1} & \dots & x_{1,6} \\ \vdots & \ddots & \vdots \\ x_{n,1} & \dots & x_{n,6} \end{bmatrix} \begin{bmatrix} h_{1,1} & \dots & h_{1,10} \\ \vdots & \ddots & \vdots \\ h_{6,1} & \dots & h_{6,10} \end{bmatrix} + \begin{bmatrix} \epsilon_{1,1} & \dots & \epsilon_{1,10} \\ \vdots & \ddots & \vdots \\ \epsilon_{n,1} & \dots & \epsilon_{n,10} \end{bmatrix} \tag{4}$$

where the matrices $\mathbf{X}_{n\times 6}$ and $\mathbf{Y}_{n\times 10}$ are the measurements calculated as described in Sec. 2.3.1 and ϵ represents the system error.

Equations (3) recursively estimate, through a predictor-corrector method, the state $\mathbf{x}_k$ and its covariance $\mathbf{P}_k$. The initial estimate of the state $\hat{\mathbf{x}}_0$ (first profile) is assumed to be known and its covariance matrix $\mathbf{P}_0$ is initialized to

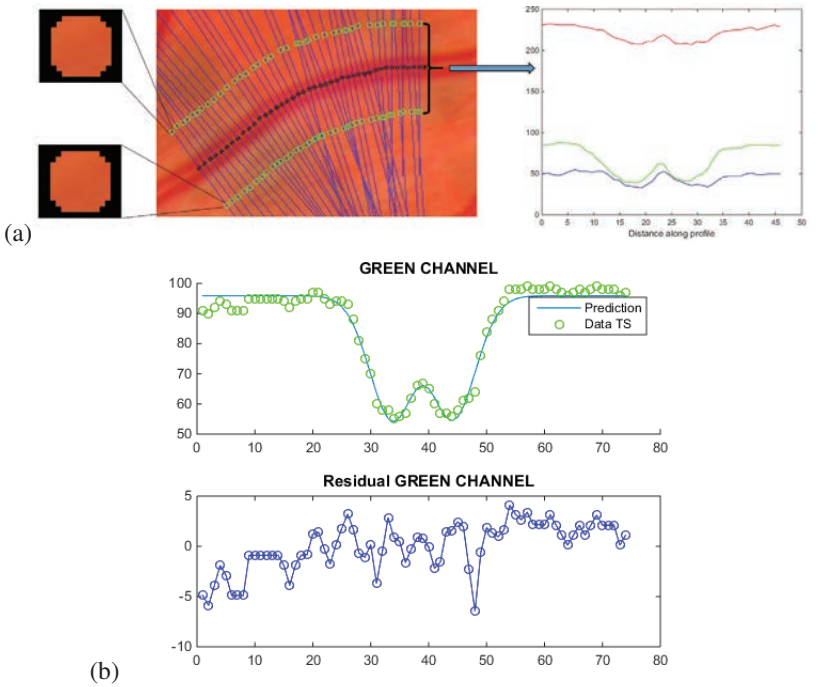

Fig. 3. (a)Cross-sections perpendicular to vessel direction, background regions and RGB intensity profile along one of the cross-sections. (b) Green channel fitting profile using the Extended Multiresolution Hermite Model.

zero. The first profile for the major arcades is the profile having background descriptors more similar to the current synthetic ones. The first profile for the branches is the profile of the parent vessel at the bifurcation point from which they originate.

Iterating this procedure, each new intensity profile of the green channel is generated taking into account the previous one and the surrounding background. A similar procedure has been developed for the red and blue channels. However, based on experimental results, we later decided to simply use the average intensity profile of the training ones for the latter two channels. The red component has been weighted with underlying background red intensity level, in order to take into account also the color spatial distribution of the whole image. Finally, the RGB intensity profile has been cut with the Full Width at Half Maximum algorithm [15] to keep the mere component of the vessel, and it has been re-sampled using the Bresenham line-drawing algorithm [16]. Experiments showed that the quality of the synthetic images generated would not improve using the full Kalman estimator in the red and blue channels.

The two vascular trees obtained, one for the arteries and one for the veins, are combined together and superimposed on synthetic backgrounds [6] to create complete synthetic fundus camera images. A Gaussian filter to smooth vessel edges, and one to reduce noise on the whole image are finally applied.

The generated synthetic image size is 3125×2336 pixels with FOV diameter of 2662 pixels, in line with the resolution of state-of-the-art fundus cameras. The whole method and a user friendly interface of the simulation tool has been implemented in Matlab®2014b. An extended dataset of synthetic images and the simulation tool will be publicly available after publication.

3. Results

In Fig. 4 we visually compare a real image (a) with two synthetic images (b, c). We notice that the synthetic vessels are characterized by a realistic morphology, including typical tortuosity. The temporal segments of the arcades go toward and around the macula, and the nasal segments radiate radially from the nerve head. The vessels colouring is always darker than the background, following real images: vessels appear brighter around the OD and darker towards the fovea and the extremities of the FOV. The arteries appear, as in real images, brighter and narrower than veins.

Because of the changes in intensity profile along the tree, the central reflex (a central, thin, bright reflection appearing sometimes along the centerline of large vessels, especially arteries) is automatically provided.

(a) 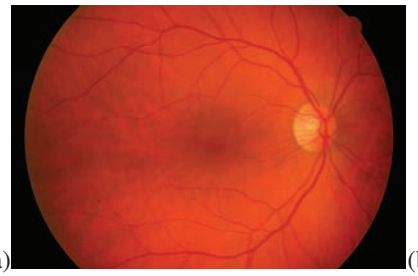 (b) 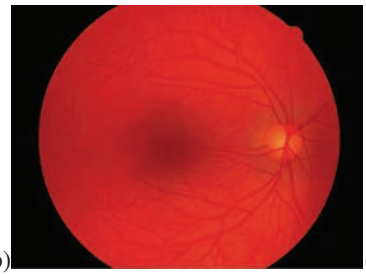 (c) 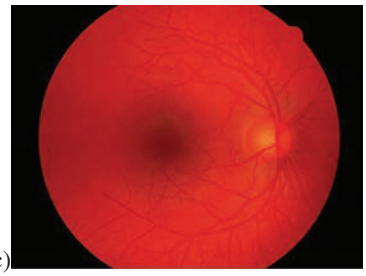

Fig. 4. Comparison between a real fundus image from the HRF dataset (a) and two complete synthetic retinal fundus images generated by our method (b,c).

In absence of quantitative quality criteria, we performed a simple qualitative assessment by asking 7 experts (ophthalmologists and researchers in retinal image analysis) to score the degree of realism of 12 synthetic retinal fundus images, using a scale from 1 to 4, where 1=not realistic at all, 2=slightly realistic, 3=nearly realistic, 4=very realistic. The best image obtained a score of 2.8, while the average score over all the images is 2.13. We did not ask the experts to make any allowance for the fact that many characteristics of fundus images are not modelled (e.g. small capillaries, the vascular network inside the OD). Considering this, the scores suggest that our synthetic images are plausible, as far as the only features generated go. The experts also suggested some improvements: the density of the vessels in some zone is too high, the largest vessels occasionally end abruptly, some first level branches appear too straight and the direction of growth sometimes recoils. These aspects will be considered in our future work.

The main purpose of this project is to generate a synthetic dataset along its GT for validation of retinal image analysis algorithms. Such techniques have to function in the same way when applied to phantoms with synthetic GT and to real images with manual GT. To demonstrate the suitability of our dataset for this purpose, we compared the performance of an automatic segmentation algorithm. The segmentation is performed with the VAMPIRE software suite [17] on 10 healthy HRF images provided manual GT and on 10 of our synthetic images having synthetic binary maps. Segmentation results are evaluated in term of the standard statistical criteria [3]. The comparison of these 2 experiments, summarized in Table 1, shows that our synthetic images behave comparably with real ones in term of vasculature segmentation and certainly in line with the performance of algorithms reported recently in the literature [18]. We note generally small differences between all values.

Table 1. Performance comparison of VAMPIRE segmentation algorithm on real (HRF) and synthetic images: True Positive Rate (TPR), False Positive Rate (FPR), Specificity (Sp), Accuracy (Acc) (mean ± std).

	TPR	FPR	Sp	Acc
Real Images	0.9874 ± 0.0015	0.0058 ± 0.0070	0.9942 ± 0.0070	0.9936 ± 0.0063
Synthetic Images	0.9703 ± 0.0185	0.0151 ± 0.0125	0.9849 ± 0.0125	0.9835 ± 0.0122

4. Conclusions

This paper has presented a novel technique to generate a reliable synthetic retinal vasculature, as part of an ongoing project aimed to generate full, realistic, synthetic fundus camera images. The results are promising for both the morphology and the texture of the vessel networks. To our best knowledge no similar method has been reported in the literature. The encouraging quality of our initial results is supported by so far small-scale visual inspection and quantitative experiments. Further improvements to this preliminary work will take into account further properties of real fundus images, including the geometric interaction between arteries and veins, the way vessels radiate from the OD, the vascular network inside the OD and the appearance of further structures like small capillaries and the retinal nerve fibre layer. An interesting future direction would be the generation of data to simulate individuals with known medical conditions.

References

1. Yin, Y., Adel, M., Bourennane, S.. Retinal vessel segmentation using a probabilistic tracking method. *Pattern Recognition* 2012;**45**(4):1235–1244.
2. Annunziata, R., Garzelli, A., Ballerini, L., Mecocci, A., Trucco, E.. Leveraging multiscale hessian-based enhancement with a novel exudate inpainting technique for retinal vessel segmentation. *IEEE Journal of Biomedical and Health Informatics* 2015;In press.
3. Trucco, E., Ruggeri, A., Karnowski, T., et al. Validating retinal fundus image analysis algorithms: Issues and a proposal. *Investigative Ophthalmology & Visual Science* 2013;**54**(5):3546–3559.
4. Collins, D.L., Zijdenbos, A.P., Kollokian, V., Sled, J.G., Kabani, N.J., Holmes, C.J., et al. Design and construction of a realistic digital brain phantom. *IEEE Transactions on Medical Imaging* 1998;**17**(3):463–468.
5. Lehmussola, A., Ruusuvuori, P., Selinummi, J., Huttunen, H., Yli-Harja, O.. Computational Framework for Simulating Fluorescence Microscope Images With Cell Populations. *IEEE Transactions on Medical Imaging* 2007;**26**(7):1010–1016.
6. Fiorini, S., Ballerini, L., Trucco, E., Ruggeri, A.. Automatic generation of synthetic retinal fundus images. In: *Medical Image Understanding and Analysis (MIUA)*. 2014, p. 7–12.
7. Odstrcilik, J., Kolar, R., Budai, A., et al. Retinal vessel segmentation by improved matched filtering: evaluation on a new high-resolution fundus image database. *IET Image Processing* 2013;**7**(4):373–383.
8. Cootes, T.F., Taylor, C.J., Cooper, D.H., Graham, J.. Active shape models-their training and application. *Computer vision and image understanding* 1995;**61**(1):38–59.
9. Trucco, E., Ballerini, L., Relan, D., et al. Novel VAMPIRE algorithms for quantitative analysis of the retinal vasculature. In: *Proc. IEEE ISSNIP/BRC*. 2013, p. 1–4.
10. Murray, C.D.. The Physiological Principle of Minimum Work Applied to the Angle of Branching of Arteries. *The Journal of General Physiology* 1926;**9**(6):835–841.
11. Lupascu, C.A., Tegolo, D., Trucco, E.. Accurate estimation of retinal vessel width using bagged decision trees and an extended multiresolution Hermite model. *Medical Image Analysis* 2013;**17**(8):1164–1180.
12. Poletti, E., Veronese, E., Calabrese, M., Bertoldo, A., Grisan, E.. Supervised classification of brain tissues through local multi-scale texture analysis by coupling dir and flair mr sequences. vol. 8314. 2012, p. 83142T–83142T–7.
13. Haralick, R.M.. Statistical and structural approaches to texture. *Proceedings of the IEEE* 1979;**67**(5):786–804.
14. Kalman, R.E.. A new approach to linear filtering and prediction problems. *Transactions of the ASME–Journal of Basic Engineering* 1960;**82**(Series D):35–45.
15. Lowell, J., Hunter, A., Steel, D., Basu, A., Ryder, R., Kennedy, R.. Measurement of Retinal Vessel Widths From Fundus Images Based on 2-D Modeling. *IEEE Transactions on Medical Imaging* 2004;**23**(10):1196–1204.
16. Bresenham, J.E.. Algorithm for computer control of a digital plotter. *IBM Syst J* 1965;**4**(1):25–30.
17. Trucco, E., Giachetti, A., Ballerini, L., Relan, D., Cavinato, A., MacGillivray, T.. Morphometric Measurements of The Retinal Vasculature in Fundus Images with Vampire. In: Lim, J.H., Ong, S.H., Xiong, W., editors. *Biomedical Image Understanding, Methods and Applications*. John Wiley & Sons, Inc; 2015, p. 91–111.
18. Fraz, M., Remagnino, P., Hoppe, A., Uyyanonvara, B., Rudnicka, A., Owen, C., et al. Blood vessel segmentation methodologies in retinal images: A survey. *Computer Methods and Programs in Biomedicine* 2012;**108**(1):407–433.